Nucleic Acids Research, 2001, Vol. 29, No. 11 ***2401–2408***

Association of an RNA kissing complex analyzed using 2-aminopurine fluorescence

Manuela J. Rist and John P. Marino*

Center for Advanced Research in Biotechnology of the University of Maryland and the National Institute for Standards and Technology, 9600 Gudelsky Drive, Rockville, MD 20850, USA

Received December 6, 2000; Revised March 21, 2001; Accepted March 29, 2001

ABSTRACT

The fluorescent probe, 2-aminopurine-2′-*O*-methyl riboside (2-AP) has been selectively incorporated at adenosine positions in stem–loops (so called R1inv and R2inv), derived from the *ColE1* plasmid encoded RNA I and RNA II transcripts, that interact to form stable loop–loop kissing complexes and bind the RNA one modulator (Rom) protein, such that fluorescence-detected stopped-flow and equilibrium methods could be used to study the detailed mechanism of this RNA–RNA interaction. Formation of loop–loop kissing complexes between R1inv and R2inv hairpins, substituted with 2-AP at positions in the complementary loops, results in a 5–10-fold fluorescence emission decrease (F_{max} = 370 nm), which provides a sensitive measure for the binding reaction. The 2-AP substituted complexes are found to have equilibrium binding properties (average K_D = 2.6 ± 1.7 nM) and affinity for Rom (average K_D = 60 ± 24 nM) that are similar to complexes formed with equivalent unlabeled hairpins. Using stopped-flow experiments, it was found that the 2-AP probes experienced at least three different microenvironments during association of the RNA complex, thus suggesting a kinetic intermediate in the kissing pathway. In contrast, dissociation of the complex was found to fit a single exponential decay (average k_{off} = 8.9 × 10^{-5} s^{-1}). Consistent with these observations, a two-step mechanism for RNA loop–loop complex association is proposed in which the complementary loops of R1inv and R2inv first base pair to form the loop–loop helix (average k_1 = 0.13 $\mu M^{-1}s^{-1}$) in the initial encounter reaction, and subsequently isomerize to the final tertiary fold in a second slower step (average k_2 = 0.09 s^{-1}), where the helical stacking around the junctions is optimized.

INTRODUCTION

In *ColE1*, the plasmid-encoded RNA II transcript acts as the primer for plasmid replication, while RNA I, a shorter plasmid-encoded transcript, which is antisense to the 5′ portion of RNA II, acts as a kinetically controlled suppressor of replication. Hybridization between RNA I and RNA II alters the conformation of RNA II and results in failure of RNaseH processing at the replication origin, thus preventing initiation of plasmid replication (1,2). In the multi-step folding pathway proposed for binding of RNA I to RNA II, a loop–loop kissing interaction between the two RNAs forms as a critical folding intermediate that holds the RNA molecules in close proximity to allow complete hybridization of RNA I to the 5′ terminus of RNA II (3–6). The plasmid-encoded RNA one modulator (Rom) protein enhances the stability of the intermediate RNA I and RNA II loop–loop complex, and thus acts as an auxiliary repressor of replication (7,8). Previous studies have demonstrated that individual hairpins derived from the RNA I and RNA II transcripts can interact with remarkable stability, with dissociation constants as low as 10^{-10} M (8–10). It has also been demonstrated that the addition of Rom protein stabilizes the loop–loop complex to dissociation and thereby increases the RNA complex lifetime by about two orders of magnitude (7–9). The high resolution solution structure of a loop–loop complex formed by enhanced stability RNA I and RNA II inverted loop sequence hairpins (so called R1inv and R2inv) has been determined using NMR spectroscopy (11,12). The NMR structure revealed that the complex formed via Watson–Crick base pairing of all seven complementary loop nucleotides thereby making a loop–loop helix which was 3′ stacked between the two stem helices (Fig. 1). The resulting pseudo-contiguously stacked helical structure showed a pronounced bend towards a compressed major groove of the loop–loop helix.

In this study, the fluorescent probe, 2-aminopurine-2′-*O*-methyl riboside (2-AP) has been selectively incorporated at adenosine positions in the sequence of stem–loops R1inv and R2inv (Fig. 1), such that fluorescence-detected stopped-flow and equilibrium methods could be used to study the detailed mechanism of this RNA kissing interaction. Substitution of 2-AP at adenosine positions in the complementary loops of R1inv and R2inv yielded constructs that retained the ability to form loop–loop complexes with native-like affinity (average K_D = 2.6 ± 1.7 nM) and bind specifically to the Rom protein (average K_D = 60 ± 24 nM). 2-AP probes act as extremely sensitive reporters for the RNA–RNA association since the fluorescence of 2-AP is highly quenched when it is stacked with other bases, but increases as much as 100-fold when fully exposed to solvent (13,14). In addition, 2-AP can form a base

*To whom correspondence should be addressed. Tel: +1 301 738 6160; Fax: +1 301 738 6255; Email: marino@carb.nist.gov

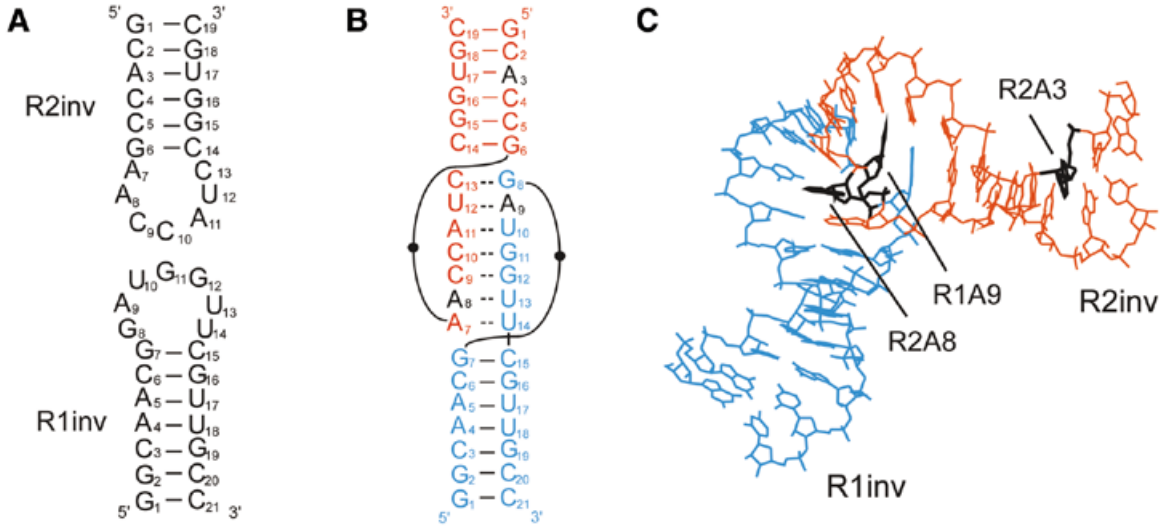

Figure 1. (**A**) RNA sequences of the stem–loop hairpins derived from the *ColE1* plasmid-encoded RNA I and RNA II transcripts (so called R1inv and R2inv). (**B**) Base pairing found in the antisense R1inv–R2inv loop–loop complex formed by these hairpins. The R2inv sequence is shown in red letters and the R1inv sequence in blue letters. Intramolecular base pairs are indicated by solid lines and intermolecular base pairs are indicated by dashed lines. Nucleotide positions in R2inv (A3 and A8) and in R1inv (A9) that were substituted with the fluorescent probe 2-AP in this study are shown in black. (**C**) Stick representation of the NMR-determined structure of the R1inv–R2inv loop–loop complex, with the sequence of R1inv in blue, the sequence of R2inv in red and the 2-AP substituted residues in black.

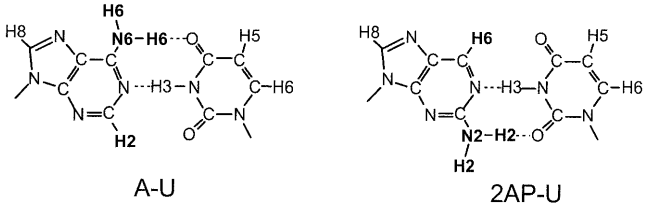

Scheme 1. Comparison of the Watson–Crick adenosine (6-aminopurine)–uracil (A-U) base pair with the 2-aminopurine-uracil (2AP-U) base pair. The H2/H6 protons and amino groups on each purine are shown in bold.

pair with uracil (Scheme 1) which is isosteric with a Watson–Crick AU base pair (13). Thus, the formation and stacking of 2AP-U base pairs during the loop–loop complex binding reaction results in a 5–10 fold fluorescent quench. Using equilibrium and real time kinetic data measured with 2-AP fluorescence, a two-step mechanism for RNA loop–loop complex association is proposed in which the complementary loops of R1inv and R2inv first form the loop–loop helix in the initial encounter reaction and subsequently isomerize to the final tertiary fold in a second slower step.

MATERIALS AND METHODS

Materials

All buffers and reagents were of the highest quality commercially available and were used without further purification.

Certain commercial equipment, instruments, and materials are identified in this paper in order to specify the experimental procedure. Such identification does not imply recommendation or endorsement by the National Institute of Standards and Technology, nor does it imply that the material or equipment identified is necessarily the best available for the purpose.

RNA and Rom synthesis

The R1inv 21mer and R2inv 19mer hairpins (Fig. 1), derived from *ColE1* plasmid-encoded RNA I and RNA II transcripts, were prepared by *in vitro* T7 polymerase run-off transcription using a synthetic DNA oligonucleotide template according to the method of Milligan and co-workers (16). DNA templates were purchased from Integrated DNA Technologies (Coralville, IA) and purified using preparative-scale denaturing PAGE. 2-AP-containing RNA oligonucleotides were synthesized on an Applied Biosystems 390 synthesizer (Perkin-Elmer, Forest City, CA) using standard phosphoramidite chemistry (17). Nucleoside phophoramidites were purchased from Glen Research (Sterling, VA). Post-synthesis base deprotection of the RNA oligonucleotides was carried out for 3 h at 55°C using a 3:1 mixture (v/v) of ammonia:methanol. The RNA oligonucleotides were then dried under nitrogen, resuspended in 1 M solution tetra-*n*-butyl ammonium fluoride (TBAF) in THF and stirred for 24 h for desilylation. Three 2-AP-labeled RNA hairpin constructs were used in this study: one 2-AP-labeled R1inv construct labeled at the A9 loop position (R1inv-9AP) and two 2-AP-labeled R2inv constructs labeled at the stem A3 (R2inv-3AP) and at the loop A8 (R2inv-8AP) positions, respectively. All RNA oligonucleotides were purified using preparative-scale denaturing polyacrylamide gel electrophoresis (PAGE) and recovered by electrophoretic elution. RNA samples were desalted and exchanged into standard buffer (1 mM cacodylate pH 6.5, 25 mM NaCl) by dialysis using a microdialysis system (Pierce Instruments, Rockford, IL). RNA concentrations were determined by measuring the absorbance at 260 nm using an extinction coefficient of 201.8 $mM^{-1}cm^{-1}$ for R1inv and 175.8 $mM^{-1}cm^{-1}$ for R2inv. The Rom protein was overexpressed and purified as described previously (18), and its concentration determined from its circular dichroism (CD) magnitude at 220 nm.

Native gel electrophoresis and UV melts

Formation of complexes by R1inv and R2inv hairpins containing 2-AP, and binding of these complexes by Rom was assayed using native PAGE. RNA was visualized by ethidium bromide staining. Binding reactions (10 µl) were performed in 1× TBM buffer (90 mM Tris pH 7.5, 90 mM boric acid, 1.0 mM $MgCl_2$). Samples were incubated for 10 min, then 10 µl aliquots were loaded on a non-denaturing 20% polyacrylamide gel (75:1 acrylamide:bisacrylamide) and run in 1× TBM buffer at 4°C at 10 V/cm using a Bio-Rad Minigel apparatus. Optical absorbance melting curves were measured on a CARY300 spectrometer (Varian Instruments, Palo Alto, CA). R1inv and R2inv hairpins were mixed at 1:1 stoichiometry in a buffer containing 10 mM cacodylate pH 6.5, 50 mM NaCl, 5.0 mM $MgCl_2$. Melting experiments were performed by heating from 10 to 90°C at a rate of 0.25°C/min, with data recorded every 1.0°C.

Steady state fluorescence measurements of RNA loop–loop complex formation and Rom binding

The fluorescence of RNA oligonucleotide samples selectively labeled with 2-AP was measured at 25°C on a SPEX Fluoromax-2 spectrofluorometer (Instruments SA, Edison, NJ) using a 0.3 cm square cuvette in 150 µl standard buffer solution (25 mM NaCl, 1 mM cacodylate pH 6.5) with 5 mM $MgCl_2$ added. Emission spectra were recorded over the wavelength range of 330–450 nm with an excitation wavelength of 310 nm. The spectral band pass was 5 nm for spectra collected at 100 nM RNA concentrations and 7 nm for spectra collected at 25 nM RNA concentration. The dissociation constant for R1inv binding to R2inv-8AP was determined by following the decrease in fluorescence (F) at 370 nm as a fixed concentration of the fluorescent RNA was titrated with increasing amounts of R1inv. Similarly, binding of R2inv to R1inv was monitored using the change in 2-AP fluorescence as a fixed concentration of R1inv-9AP was titrated with increasing amounts of the R2inv. The RNA–RNA binding in each case was fitted using a single-site equilibrium binding equation. For example, single-site binding of R2inv to R1inv-9AP was fit as follows:

$$F = -\{(F_0 - F_f)/2[\text{R1inv - 9AP}]_{tot}\}\left\{b - \sqrt{b^2 - (4[\text{R2inv}]_{tot}[\text{R1inv - 9AP}]_{tot})}\right\} + F_0 \quad \mathbf{1}$$

where $b = K_D + [\text{R2inv}]_{tot} + [\text{R1inv-9AP}]_{tot}$, F_o and F_f are the initial and final fluorescence intensities, respectively, $[\text{R2inv}]_{tot}$ is the total concentration of R2inv, and $[\text{R1inv-9AP}]_{tot}$ is the total R1inv-9AP concentration.

The dissociation constant for Rom binding to the RNA inverted loop–loop complex was determined by following the decrease in fluorescence at 370 nm as a fixed concentration of R1inv-9AP and R2inv, mixed in 1:1 stoichiometry in standard buffer containing 30 mM $SrCl_2$, was titrated with Rom. At this concentration of $SrCl_2$, 100% RNA loop–loop complex was observed so that the binding data could be fitted using a single-site binding mode for Rom according to equation **2**:

$$F = -\{(F_0 - F_f)/2[\text{R2} \cdot \text{R1-9AP}]_{tot}\}\left\{b - \sqrt{b^2 - (4[\text{Rom}]_{tot}[\text{R2} \cdot \text{R1-9AP}]_{tot})}\right\} + F_0 \quad \mathbf{2}$$

where $b = K_D + [\text{Rom}]_{tot} + [\text{R2}\cdot\text{R1-9AP}]_{tot}$, $[\text{R2}\cdot\text{R1-9AP}]_{tot}$ is the total R2inv·R1inv-9AP concentration, and $[\text{Rom}]_{tot}$ is the total concentration of Rom protein. Rom contains no tryptophan residues, therefore no correction had to be applied to remove a fluorescence contribution from the protein. All binding data were collected at 25°C.

Measurement of binding kinetics

To determine the kinetics of RNA loop–loop complex formation, stopped-flow fluorescence experiments were performed at 25°C in standard buffer solution with 5 mM $MgCl_2$ using a stopped-flow device from Applied Photophysics (Surrey, UK) in the two-syringe mode (dead time = 1.1 ms). The kinetics of RNA complex formation was followed using pseudo-first-order conditions, where the R2inv was present at concentrations from 5 to 25-fold greater than the R1inv-9AP. The time course of the decrease in 2-AP fluorescence (F_t) as a result of loop–loop complex formation showed two kinetic phases and was fit to the double exponential expression, $F_t = [F_1\exp(-k_1t)] + [F_2\exp(-k_2t)] + C$ where F_1, F_2 and k_1, k_2 are the amplitudes and rate constants for the first and second kinetic phases, respectively, and C is a constant offset. In these experiments, the R1inv-9AP was excited at 310 nm, and the fluorescence was monitored using a 360 nm cut-off filter.

The concentration dependence of the observed rates of binding was fit using the simple two-step binding mechanism of equation **3**:

$$\text{R1inv} + \text{R2inv} \Leftrightarrow \text{R1inv} \cdot \text{R2inv} \Leftrightarrow \text{R1inv} \cdot \text{R2inv}^* \quad \mathbf{3}$$

The concentration dependent rates of the reaction, showing linear and hyperbolic dependent curves, were fitted using the program KaleidaGraph (Synergy Software). The linearly dependent rate was fit to the equation $k_{obs} = k_1[\text{R2inv}] + (k_{-1} + k_2 + k_{-2})$ with the slope defining the second-order rate constant and the intercept giving an estimate of the overall dissociation rates, $k_{-1} + k_2 + k_{-2}$. The maximal rate ($k_{max} = k_2 + k_{-2}$) was estimated from the maximum of the hyperbolic dependent rate. Since $(k_{-1} + k_{-2}) << k_2$, k_2 was estimated by assuming k_{-1} and k_{-2} were equal to zero in these equations. Due to the extremely slow rates (estimated to be $<10^{-2}$ s^{-1}), k_{-1} and k_{-2} could not be determined explicitly from fitting the curves. However, using the measured k_{off}, the product $k_{-2}k_{-1}$ could be determined from the simplified equation $(k_{-2}k_{-1})/k_2$ and the equilibrium constant K_D^{calc} calculated using k_2, k_1 and $k_{-2}k_{-1}$.

The dissociation of the loop–loop complex was measured using the SPEX Fluoromax-2 spectrofluorometer by following the increase in 2-AP fluorescence of either R2inv-8AP or R1inv-9AP as the RNA complex dissociated. The reaction was carried out in standard buffer solution with 5 mM $MgCl_2$ and made irreversible by trapping either the free R1inv or R2inv, respectively, with a 20-fold excess of unlabeled complementary RNA hairpin added manually, thereby preventing rebinding of the dissociated hairpin to the 2-AP-labeled complement. The time course was fitted using first order rate, $F_t = F_1[1 - \exp(-k_1t)] + C$, where k_1 is the observed off-rate for the complex.

Error analysis

The reported errors are the standard uncertainties of the data from the best-fit theoretical curves. This method assumes that the standard uncertainty of the measurement is approximated

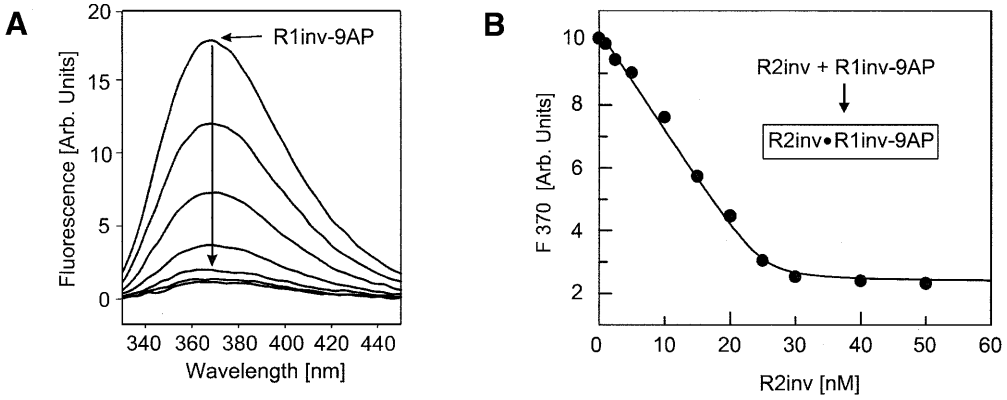

Figure 2. Fluorescence changes accompanying titration of 2-AP-labeled R1inv-9AP with R2inv. (**A**) Fluorescence emission spectra from 330 to 450 nm as a function of titration of 100 nM R1inv-9AP with increasing concentrations of R2inv in standard buffer (25 mM NaCl, 1 mM cacodylate pH 6.5, 5 mM $MgCl_2$) at 25°C. (**B**) Plot of the relative fluorescence decrease at 370 nm as a function of total R2inv concentration for a titration using 25 nM R1inv-9AP. The solid curve is a fit to equation **1** ($K_D = 0.23 \pm 0.19$ nM). The species that is directly detected in the experiment is marked within the box.

Table 1. Kinetic rates and thermodynamic binding constants

RNA constructs	K_D [RNA·RNA] (nM)	K_D [RNA·Rom] (nM)	$k_{off} \times 10^{-5}$ (s^{-1})	k_1 ($\mu M^{-1}s^{-1}$)	k_2 (s^{-1})	$k_{-1}k_{-2}$ (s^{-2})	K_D^{calc} (nM)
R1inv-9AP + R2inv	1.6 ± 1.1	56 ± 26	8.2 ± 0.03	0.12 ± 0.012	0.09 ± 0.03	7.3×10^{-6}	0.68
R2inv-8AP + R1inv	3.6 ± 2.2	64 ± 22	9.7 ± 0.01	0.14 ± 0.008	0.09 ± 0.04	7.7×10^{-6}	0.61

Measurements were made in the standard buffer at 25°C. The thermodynamic parameters represent average values from different experiments, and the errors are standard uncertainties. The kinetic constants correspond to the two-step binding mechanism in equation **3**. The equilibrium constant K_D for the RNA loop–loop complex formation was calculated from the kinetic constants (i.e. $K_D^{calc} = k_{-1}k_{-2}/k_1k_2$).

by the standard deviation of the points from the fitted curve (19).

RESULTS

RNA complex formation and Rom binding

Incorporation of single 2-AP probes at naturally occurring adenosine positions of the R1inv and R2inv hairpins (Fig. 1) provided sensitive probes for measurement of RNA loop–loop complex equilibrium binding and real time kinetic measurements. To confirm independently of the fluorescence measurements that no structural perturbation resulted from substitution of 2-AP probes in R1inv and R2inv, native gel electrophoresis and UV-melting analysis were performed using the 2-AP constructs. For all 2-AP RNA constructs used in this study, stable complexes could be observed, that were super-shifted by Rom protein, under identical native gel conditions used to observe RNA complex formation and Rom binding of the unlabeled hairpins (data not shown). In addition, UV-melting curves measured for loop–loop complexes formed by the 2-AP RNA constructs were practically indistinguishable from melts of unlabeled complexes, with approximately the same T_ms observed for loop–loop (T_m ~65°C) and hairpin (T_m > 85°C) helix melting transitions in all cases.

In Figure 2A, it is shown that the intensity of the 2-AP emission spectrum of R1inv-9AP construct is initially relatively high and decreases in a saturable fashion as the concentration of R2inv is increased, with a maximal decrease of ~5-fold. The direction of the fluorescence change indicates that the 9AP-substituted base becomes stacked upon binding to R2inv, which is consistent with the formation of a R1A9–R2U12 base pair as observed in the NMR structure (11,12) of the inverted loop–loop complex (Fig. 1). In this experiment and all further RNA titrations discussed, formation of the loop–loop complex absolutely required the presence of divalent cations in the reaction buffer. In contrast, titration of the RNA hairpins with monovalent cations resulted in no significant change in fluorescence emission at 370 nm up to a concentration of 1.0 M, indicating that the loop–loop complex is not stabilized by monovalent cations. By fitting the data shown in Figure 2 to equation **1**, a $K_D = 0.23 \pm 0.19$ nM for RNA loop–loop complex formation at 25°C was calculated (note that the precision of determined K_Ds was lower for certain experiments due to the fact that reactions were measured at concentrations that approximated stoichiometric binding conditions). In additional measurements in which the R1inv-9AP concentration was varied from 25 to 100 nM (n = 2), an average K_D value of 1.6 ± 1.1 nM for RNA loop–loop complex formation was determined.

The formation of the RNA loop–loop complex could also be monitored using the intensity of the 2-AP emission spectrum of the R2inv-8AP RNA hairpin construct as a function of R1inv concentration. For the R2inv-8AP hairpin, the 2-AP emission spectrum is also initially relatively high and decreases in a saturable fashion as the concentration of R1inv is increased (data not shown). As observed for the R1inv-9AP construct, the direction of the fluorescence change indicates

that 2-AP probes become stacked upon binding to R1inv, which is again consistent with the NMR structure of the loop–loop complex. By fitting the data to equation **1**, average K_D = 3.6 ± 2.2 nM for RNA loop–loop complex formation at 25°C was calculated. In contrast with these two 2-AP RNA hairpin constructs, a control hairpin with the 2-AP label placed in the stem (R2inv-3AP) showed an initially highly quenched state in the hairpin alone and produced no appreciable fluorescence change upon titration with R1inv (data not shown). This confirms that the principle reason for quenching of the 2-AP probes placed in the complementary loops is due to the formation of the loop–loop helix upon RNA–RNA association and that stacking of the stem base pairs is not significantly perturbed when the complex forms.

The average K_D measured and calculated here using 2-AP fluorescence for the inverted RNA loop–loop complex agrees well with the K_D = 0.57 nM that was previously measured at 25°C by following the formation of enzymatic cleavage products using denaturing gel electrophoresis (8,9). The results obtained using the fluorescence measurements, together with the results of native PAGE and UV-melting analysis, therefore demonstrate that 2-AP probes do not significantly affect RNA complex formation and can act as sensitive reporters for complex formation. The K_Ds determined using the different 2-AP RNA constructs are summarized in Table 1.

Figure 3A shows a trace of the 2-AP emission spectrum of R1inv-9AP mixed with R2inv in the absence of any divalent metal ion, in the presence of 30 mM $SrCl_2$ and after titration with a saturable quantity of Rom protein. The addition of Rom protein to the RNA complex formed in the presence of 30 mM $SrCl_2$ resulted in a further decrease in the 2-AP fluorescence of R2inv·R1inv-9AP in a saturable fashion, with a maximal decrease of ~25% of the original fluorescence. The direction of the fluorescence change indicates that 2-AP becomes more stacked upon binding of Rom, which is consistent with stabilization and further bending of the RNA loop–loop complex by Rom that has been previously observed. By fitting the data shown in Figure 3B to equation **2**, a K_D = 64 ± 22 nM for Rom binding to the RNA loop–loop complex at 25°C was calculated. These results (Table 1) indicate that RNA complexes formed with the 2-AP construct are also still able to bind specifically to the Rom protein with native-like affinity.

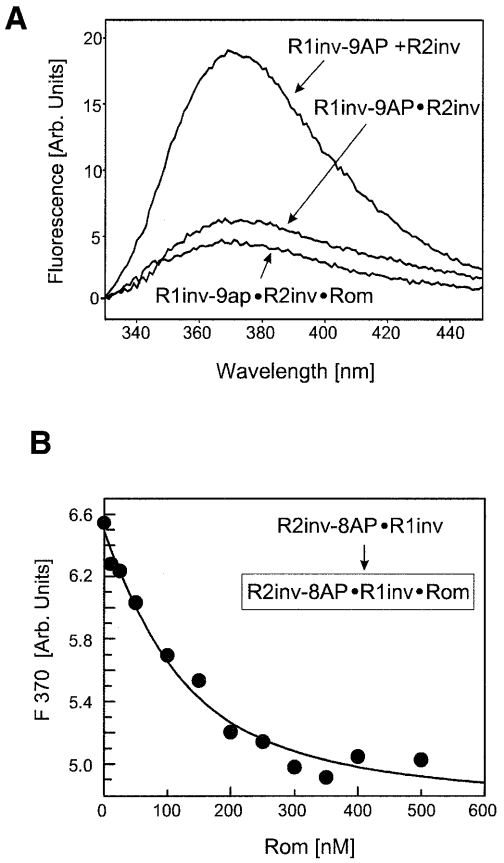

Figure 3. Fluorescence changes accompanying titration of the RNA loop–loop complex formed between R1inv and R2inv in the presence of 30 mM $SrCl_2$ with Rom. (**A**) Fluorescence emission spectra from 330 to 450 nm of the 1:1 stoichiometric mixture of R1inv-9AP and R2inv in standard buffer (R1inv-9AP + R2inv), with 30 mM $SrCl_2$ added (R1inv-9AP·R2inv), and after titration with Rom is completed (R1inv-9AP·R2inv·Rom). Note that at this concentration of Sr^{2+}, 100% RNA loop–loop complex was observed so that the binding data could be fitted using a single-site binding mode for Rom according to equation **2**. (**B**) Plot of the relative fluorescence decrease at 370 nm accompanying titration of 100 nM R1inv·R2inv-8AP complex with increasing concentrations of Rom protein. The solid curve is a fit to equation **2** (K_D = 64 ± 22 nM). The species that is directly detected in the experiment is marked within the box.

Kinetic analysis of RNA kissing complex formation

Stopped-flow fluorescence detected kinetic experiments, using either 2-AP-labeled R1inv and unlabeled R2inv or 2-AP-labeled R2inv and unlabeled R1inv, indicate that the formation of the RNA inverted loop–loop complex occurs in two kinetic phases (Fig. 4A), which suggests a two-step binding mechanism. In experiments using either R1inv-9AP or R2inv-8AP constructs, one kinetic phase is found to be linearly dependent on complementary unlabeled RNA hairpin concentration, while a second phase approximately follows a hyperbolic dependence on unlabeled RNA hairpin concentration (Fig. 4B). In addition, rate constants measured using observed fluorescence changes for the 2-AP probes placed in the complementary loops of either R1inv or R2inv hairpin were found, within the error of the measurements, to be the same. Thus, the 2-AP probes appear to report on similar global folding events associated with RNA binding that are manifested in changes in the local 2-AP microenvironment. For a kinetic mechanism as described in equation **3**, the slope of the linear phase is equal to the observed on-rate, k_1, and the *y*-intercept is equal to the sum of $k_{-1} + k_{-2} + k_2$ (20). An average k_1 = 0.13 $\mu M^{-1}s^{-1}$ has been determined based on the slope of the linear phase. For the hyperbolically dependent phase, the asymptotic rate is equal to the sum $k_2 + k_{-2}$, and the *y*-intercept provides a crude estimate of the off-rate. Since $(k_{-1} + k_{-2}) << k_2$, an average k_2 of 0.09 s^{-1} was estimated by assuming k_{-1} and k_{-2} were equal to zero in these equations. Due to the extremely slow rates, k_{-1} and k_{-2} could not be determined explicitly from fitting the curves in Figure 4B and only an approximate upper limit of 10^{-2} s^{-1} can be assigned for k_{-1} and k_{-2}. Nonetheless, the product of the rate constants, $k_{-1}k_{-2}$, could be determined from the off-rate of the RNA complex, which was measured using a trapping experiment. In the off-rate experiment (Fig. 4C), a single-exponential rate is observed for the RNA complex

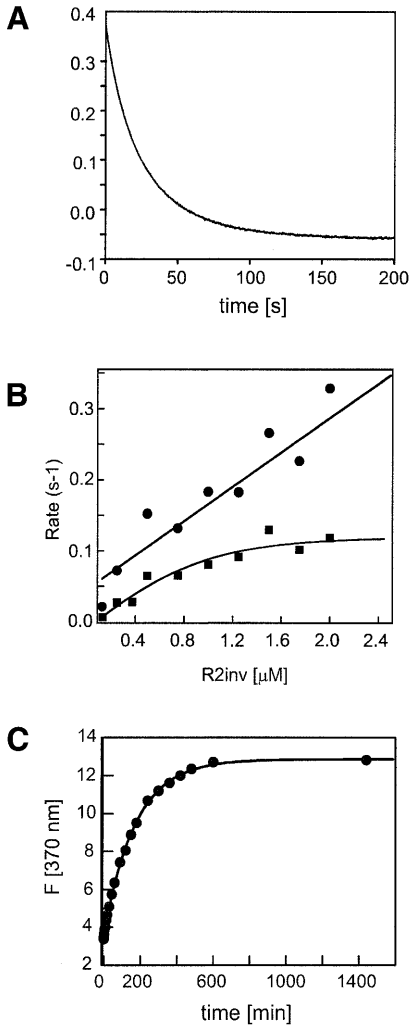

Figure 4. Kinetic measurements of RNA complex formation between R1inv and R2inv hairpins. (**A**) Stopped-flow measurement of the association rate by monitoring the fluorescence change at 370 nm upon rapid mixing of R1inv-9AP with R2inv. The representative trace was obtained at 100 nM R1inv-9AP and 500 nM R1inv concentrations and fit to a double exponential equation (k_1 = 0.013 s^{-1}, k_2 = 0.0049 s^{-1}). (**B**) Concentration dependence of the two kinetic phases of the R1inv·R2inv complex formation. The linear dependent rates are plotted as circles and the hyperbolic dependent rates as squares. (**C**) Determination of the R1inv off-rate from R2inv-8AP using unlabeled R2inv as an irreversible trap for the free R1inv. A complex consisting of 100 nM each R2inv-8AP and R1inv was rapidly mixed by hand with a solution of 2 μM R2inv. A k_{off} of 9.7×10^{-5} s^{-1} for R2inv was determined from this experiment.

dissociation with an average $k_{off} = 8.9 \times 10^{-5}$ s^{-1}. Using this measured k_{off} and the estimate for k_2, the equation $k_{off} = (k_{-1}k_{-2})/k_2$ could be fit and the product of the rate constants $k_{-1}k_{-2}$ determined (average $k_{-1}k_{-2} = 7.5 \times 10^{-6}$). The equilibrium binding constant K_D was calculated from the measured microscopic rate constants, $K_D^{calc} = k_{-1}k_{-2}/k_1k_2$, to be on average 0.65 nM, which is in good agreement with the measured K_D (average $K_D = 2.6 \pm 1.7$ nM). Thus, the two-step mechanism is consistent with the thermodynamic measurements on this RNA system. Rate constants for the two-step mechanism are reported in Table 1.

DISCUSSION

2-AP as a probe of RNA kissing interactions

2-AP has been shown in previous studies to be a useful probe of the structure and dynamics of specific sites in DNA (21–23), as a monitor for enzyme–DNA (22,24–26) and RNA–ligand interactions (27,28) and to study Mg^{2+}-dependent conformational changes in the hammerhead ribozyme (29,30). In this study, a general quantitative method is presented for studying RNA kissing complexes that uses changes in the quantum yield of 2-AP fluorescence emission. It is shown that substitution of 2-AP at positions in the complementary loops of the RNA hairpins that form kissing complexes yields constructs that retain the ability to form native-like interactions, e.g. RNA–RNA kissing and Rom binding, while acting as extremely sensitive reporters for the RNA–RNA binding reaction. The general mechanism of the fluorescence detection is based on the large quenching of the 2-AP fluorescence emission observed upon formation of 2AP-U base pairs when the RNA hairpins bind. For all R1inv and R2inv constructs used in this study with fluorescent 2-AP reporters substituted into positions in the complementary loops, formation of the complex was accompanied by a large (5–10-fold) quench in the fluorescence quantum yield of the 2-AP probe. The direction and magnitude of this fluorescence change indicates that the 2-AP-substituted base becomes significantly stacked upon binding, which is consistent with 2-AP-U base pairing that would accompany the formation of the loop–loop helix and the coaxial stacking of this helix between the two stem helices (Fig. 1). In contrast to other binding assays, like native gel electrophoresis and filter binding, the 2-AP fluorescence assay is in general more sensitive and less prone to artifacts that could produce inaccurate binding constant measurements since 2-AP probe incorporation can be non-perturbing and binding measurements can be made under native solution conditions. For example, K_Ds measured using 2-AP fluorescence for Rom protein binding to the RNA kissing complex are in good agreement with previous measurements made indirectly by quantification of the products of RNAse cleavage reactions (9); while direct measurements made using native gel electrophoresis underestimate the K_D by approximately one order of magnitude (18).

A two-step mechanism for RNA kissing

In *ColE1*, plasmid copy number is controlled kinetically and depends on the rate by which the antisense(RNA I)–target(RNA II) complex is formed rather than on binding equilibrium. A kissing interaction is the critical first step in the formation of this antisense(RNA I)– target(RNA II) complex. Understanding the details of the mechanism for how the antisense RNA I molecules targets its cognate RNA II target is therefore critical to understanding how these molecules work *in vivo*. In this study, the 2-AP fluorescence-detected fast kinetic measurements of the RNA I–RNA II kissing interaction provide the first insight into the details of this important binding reaction on a millisecond to second time scale. From the stopped-flow experiments, 2-AP probes substituted in the complementary loops of the R1inv and R2inv hairpins have been shown to experience at least three different

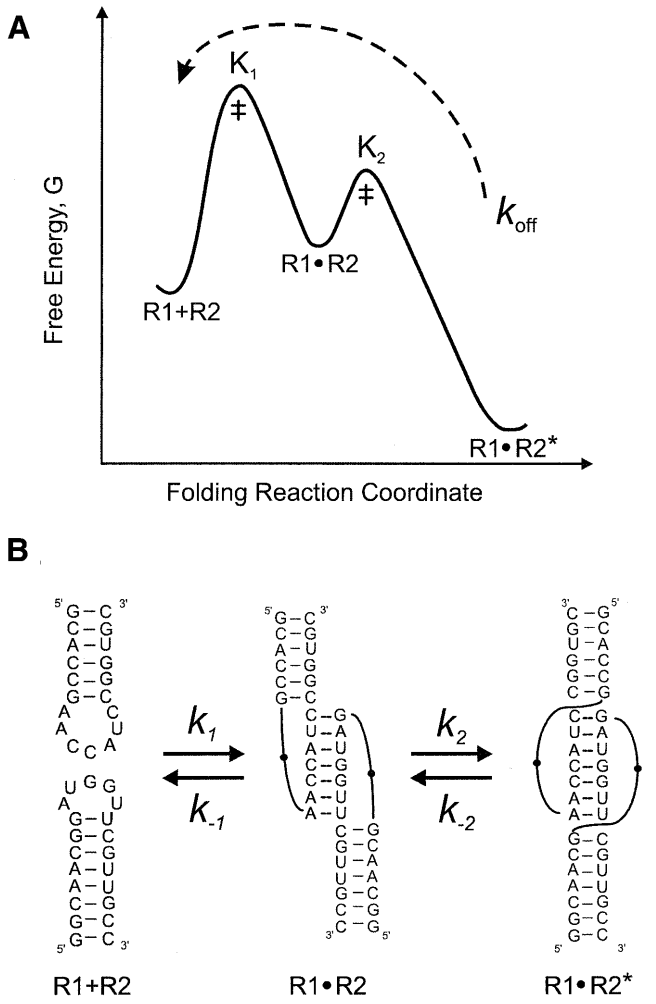

Figure 5. (**A**) Three-state model for the association of the R1inv–R2inv loop–loop kissing complex. A collision complex initially forms via loop–loop helix formation between the two individual hairpins, which is then followed by a much slower isomerization to the final tertiary fold. (**B**) Proposed model for the folding states in the association of the RNA loop–loop complex. In the initial step, the two hairpins associate to form the loop–loop helix through Watson–Crick base pairing. In the second step, the complex isomerizes to a more stable tertiary fold in which the loop–loop helix is optimally stacked between the two stem helices.

microenvironments during association of the RNA complex (Fig. 4). The simplest explanation for this observation is that the RNA kissing reaction occurs via a two-step mechanism, with a single kinetic intermediate state. The two-step mechanism for RNA loop–loop complex formation can be described as an initial encounter of the RNA hairpins in which the complementary loops of R1inv and R2inv first base pair to form the loop–loop helix (average $k_1 = 1.3 \times 10^5$ $M^{-1}s^{-1}$), and then a subsequent isomerization of the RNA complex to the final tertiary fold in a second slower step (average $k_2 = 0.09$ s^{-1}), where the helical stacking around the junctions is optimized. This three-state model for the folding trajectory for the kissing interaction is shown schematically in Figure 5. The second-order rate constant measured for the initial encounter step of the kissing interaction is in the range of values expected for formation of this type of antisense complex and is consistent with previous estimates (8,9). Since ($k_{-1} + k_{-2}$) is estimated to be much less than k_2, the folding pathway for the kissing interaction (Fig. 5A) shows energetic barriers to the backward k_{-1} and k_{-2} rates, which are significantly higher than the barrier to the forward rate, k_2. As a consequence of the relative values of k_{-1}, k_2 and k_{-2}, and the observation that k_{off} can be fit to a single first order rate, the on-rate can be estimated by k_1 (average $k_1 = 1.3 \times 10^5$ $M^{-1}s^{-1}$, Table 1) and the off-rate by $k_{-1}k_{-2}/k_2$ (average $k_{off} = 8.6 \times 10^{-5}$ s^{-1}, Table 1). Overall, the low K_D value measured and calculated for the kissing complex formation is therefore largely the result of the slow off-rate.

The significant decrease in fluorescence that occurs upon forming the initial encounter complex is consistent with 2-AP-U base pairing and stacking in the initial binding event of loop–loop helix formation (Fig. 5B). The second slower kinetic transient, which has a smaller amplitude, may represent a final isomerization step in which the RNA complex assumes its final folded conformation. Such an isomerization step may contribute significantly to the total free energy of binding of the complex since it would involve rearrangement to the optimal stacking geometry, especially at the junctions between the stem helices and the loop–loop helix. This idea is consistent with previous findings that base stacking contributes most significantly to the thermodynamic stability of RNA kissing complexes (10) and also suggests that the rate k_{-2} is likely to be significantly slower than k_{-1} in the unfolding pathway.

ACKNOWLEDGEMENTS

We thank Dr F.Song (CARB) for synthesis of the 2-AP-labeled RNA constructs, Prof. L.Regan (Yale University) for providing us with purified Rom protein, and Dr T.E.Shrader (Albert Einstein College of Medicine) for providing us with plasmid (pT7-911Q). We also thank Dr J.T.Stivers (CARB) for stimulating discussions. This work was supported by the NIH (GM 59107-01) to J.P.M. M.J.R. is a NIST Visiting Fellow.

REFERENCES

1. Eguchi,Y., Itoh,T. and Tomizawa,J. (1991) Anti-sense RNA. *Annu. Rev. Biochem.*, **60**, 631–652.
2. Tomizawa,J. (1987) In Inouye,M.D. and Dudock,B.S. (eds), *Molecular Biology of RNA, New Perspectives.* Academic Press, New York, NY, pp. 249–259.
3. Tomizawa,J. (1984) Control of ColE1 plasmid replication: the process of binding of RNA I to the primer transcript. *Cell*, **38**, 861–870.
4. Tomizawa,J. (1985) Control of ColE1 plasmid replication: initial interaction of RNA I and the primer transcript is reversible. *Cell*, **40**, 527–535.
5. Tomizawa,J. (1986) Control of ColE1 plasmid replication: binding of RNA I to RNA II and inhibition of primer formation. *Cell*, **47**, 89–97.
6. Tomizawa,J. (1990) Control of ColE1 plasmid replication: intermediates in the binding of RNA I and RNA II. *J. Mol. Biol.*, **212**, 683–694.
7. Tomizawa,J. (1990) Control of ColE1 plasmid replication: interaction of Rom protein with an unstable complex formed by RNA I and RNA II. *J. Mol. Biol.*, **212**, 695–708.
8. Eguchi,Y. and Tomizawa,J. (1990) Complex formed by complementary RNA stem–loops and its stabilization by a protein: function of ColE1 Rom protein. *Cell*, **60**, 199–209.
9. Eguchi,Y. and Tomizawa,J. (1991) Complexes formed by complementary RNA stem–loops: their formations, structures and interaction with ColE1 Rom protein. *J. Mol. Biol.*, **220**, 831–842.
10. Gregorian,R.S. and Crothers,D.M. (1994) Determinants of RNA hairpin loop–loop complex stability. *J. Mol. Biol.*, **248**, 968–984.

11. Marino,J.P., Gregorian,R.S., Csankovszki,G. and Crothers,D.M. (1995) Bent helix formation between RNA hairpins with complementary loops. *Science*, **268**, 1448–1454.
12. Lee,A. and Crothers,D. (1998) The solution structure of an RNA loop–loop complex: the ColE1 inverted loop sequence. *Structure*, **6**, 993–1005.
13. Millar,D.P. (1996) Fluorescence studies of DNA and RNA structure and dynamics. *Curr. Opin. Struct. Biol.*, **6**, 322–326.
14. Jean,J.M. and Hall,K.B. (2001) 2-Aminopurine fluorescence quenching and lifetimes: role of base stacking. *Proc. Natl Acad. Sci. USA*, **98**, 37–41.
15. Milligan,J.F. and Uhlenbeck,O.C. (1989) Synthesis of small RNAs using T7 RNA polymerase. *Methods Enzymol.*, **180**, 51–62.
16. Milligan,J.F., Groebe,D.R., Witherell,G.W. and Uhlenbeck,O.C. (1987) Oligonucleotide synthesis using T7 RNA polymerase and synthetic DNA templates. *Nucleic Acids Res.*, **15**, 8783–8798.
17. Beaucage,S.L. and Caruthers,M.H. (1981) Deoxynucleoside phosphoramidites – a new class of key intermediates for deoxypolynucleotide synthesis. *Tetrahedron Lett.*, **22**, 1859.
18. Predki,P.F., Nayak,L.M., Gottlieb,M.B. C. and Regan,L. (1995) Dissecting RNA–protein interactions: RNA–RNA recognition by Rop. *Cell*, **80**, 41–50.
19. Flannery,B.P., Teukolsky,S.A. and Vetterling,W.T. (1992) *Numerical Recipes in Fortran*., 2nd Edn. Cambridge University Press, Cambridge, UK.
20. Johnson,K.A. (1992) *The Enzymes*, Vol. XX, Academic Press, Orlando, FL.
21. Stivers,J.T. (1998) 2-Aminopurine fluorescence studies of base stacking interactions at abasic sites in DNA: metal-ion and base sequence effects. *Nucleic Acids Res.*, **26**, 3837–3844.
22. Holz,B., Klimasauskas,S., Serva,S. and Weinhold,E. (1998) 2-Aminopurine as a fluorescent probe for DNA base flipping by methyltransferases. *Nucleic Acids Res.*, **26**, 1076–1083.
23. Nordlund,T.M., Evans,K.O. and Xu,D. (1998) Conformations of DNA bases: 2-aminopurine fluorescence decays and NMR. *Biophys. J.*, **74**, A21.
24. Frey,M.W., Sowers,L.C., Millar,D.P. and Benkovic,S.J. (1995) The nucleotide analog 2-aminopurine as a spectroscopic probe of nucleotide incorporation by the Klenow fragment of *Escherichia coli* polymerase I and bacteriophage-T4 DNA-polymerase. *Biochemistry*, **34**, 9185–9192.
25. Marquez,L.A. and Reha-Krantz,L.J. (1996) Using 2-aminopurine fluorescence and mutational analysis to demonstrate an active role of bacteriophage T4 DNA polymerase in strand separation required for 3′→5′-exonuclease activity. *J. Biol. Chem.*, **271**, 28903–28911.
26. Stivers,J.T., Pankiewicz,K.W. and Watanabe,K.A. (1999) Kinetic mechanism of damage site recognition and uracil flipping by *Escherichia coli* uracil DNA glycosylase. *Biochemistry*, **38**, 952–963.
27. Lacourciere,K.A., Stivers,J.T. and Marino,J.P. (2000) Mechanism of neomycin and Rev peptide binding to the Rev responsive element of HIV-1 as determined by fluorescence and NMR spectroscopy. *Biochemistry*, **39**, 5630–5641.
28. Parrott,A.M., Lago,H., Adams,C.J., Ashcroft,A.E., Stonehouse,N.J. and Stockley,P.G. (2000) RNA aptamers for the MS2 bacteriophage coat protein and the wild-type RNA operator have similar solution behaviour. *Nucleic Acids Res.*, **28**, 489–497.
29. Menger,M., Tuschl,T., Eckstein,F. and Porschke,D. (1996) Mg^{2+}-dependent conformational changes in the hammerhead ribozyme. *Biochemistry*, **35**, 14710–14716.
30. Menger,M., Eckstein,F. and Porschke,D. (2000) Multiple conformational states of the hammerhead ribozyme, broad time range of relaxation and topology of dynamics. *Nucleic Acids Res.*, **28**, 4428–4434.